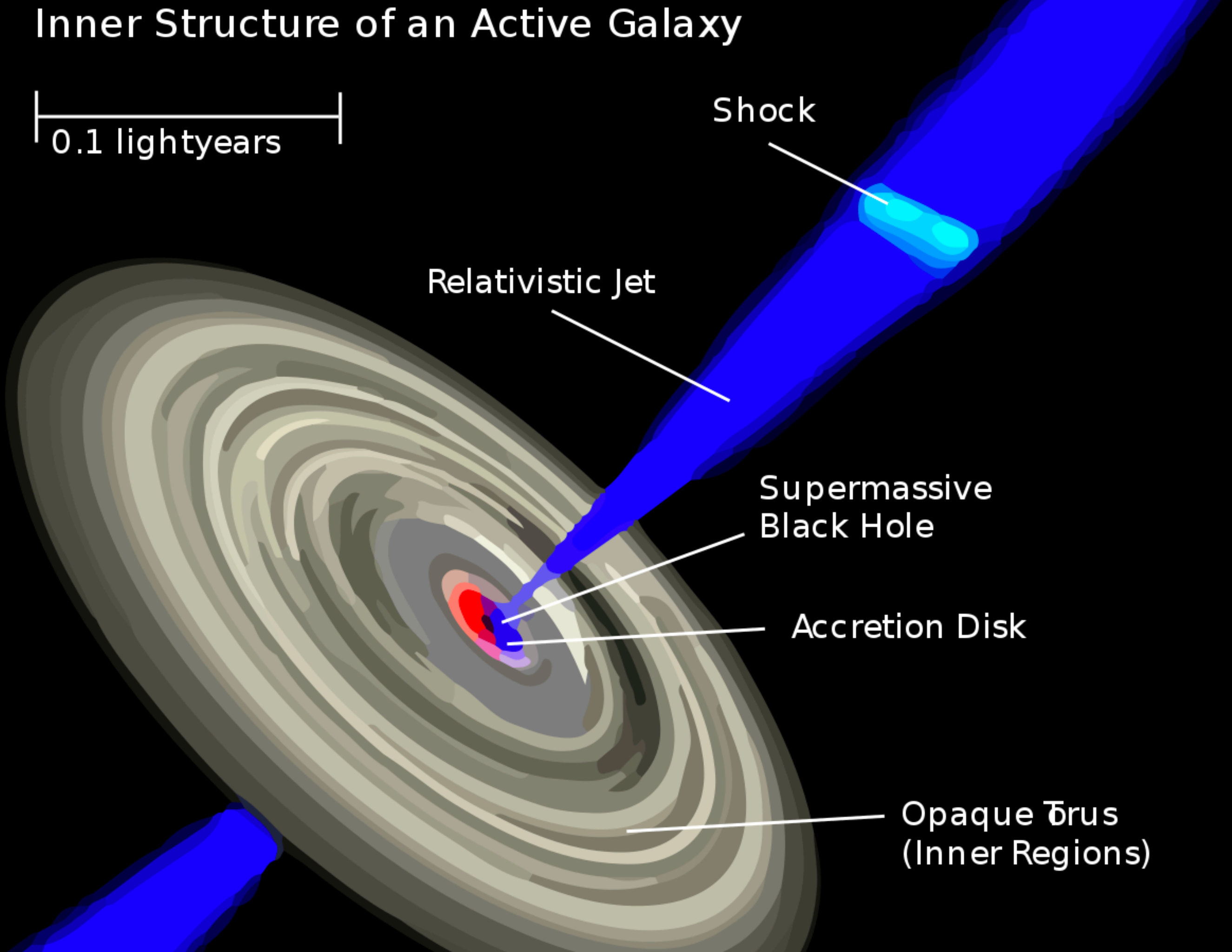


Inner Structure of an Active Galaxy

0.1 lightyears



Shock

Relativistic Jet

Supermassive Black Hole

Accretion Disk

Opaque Turb (Inner Regions)

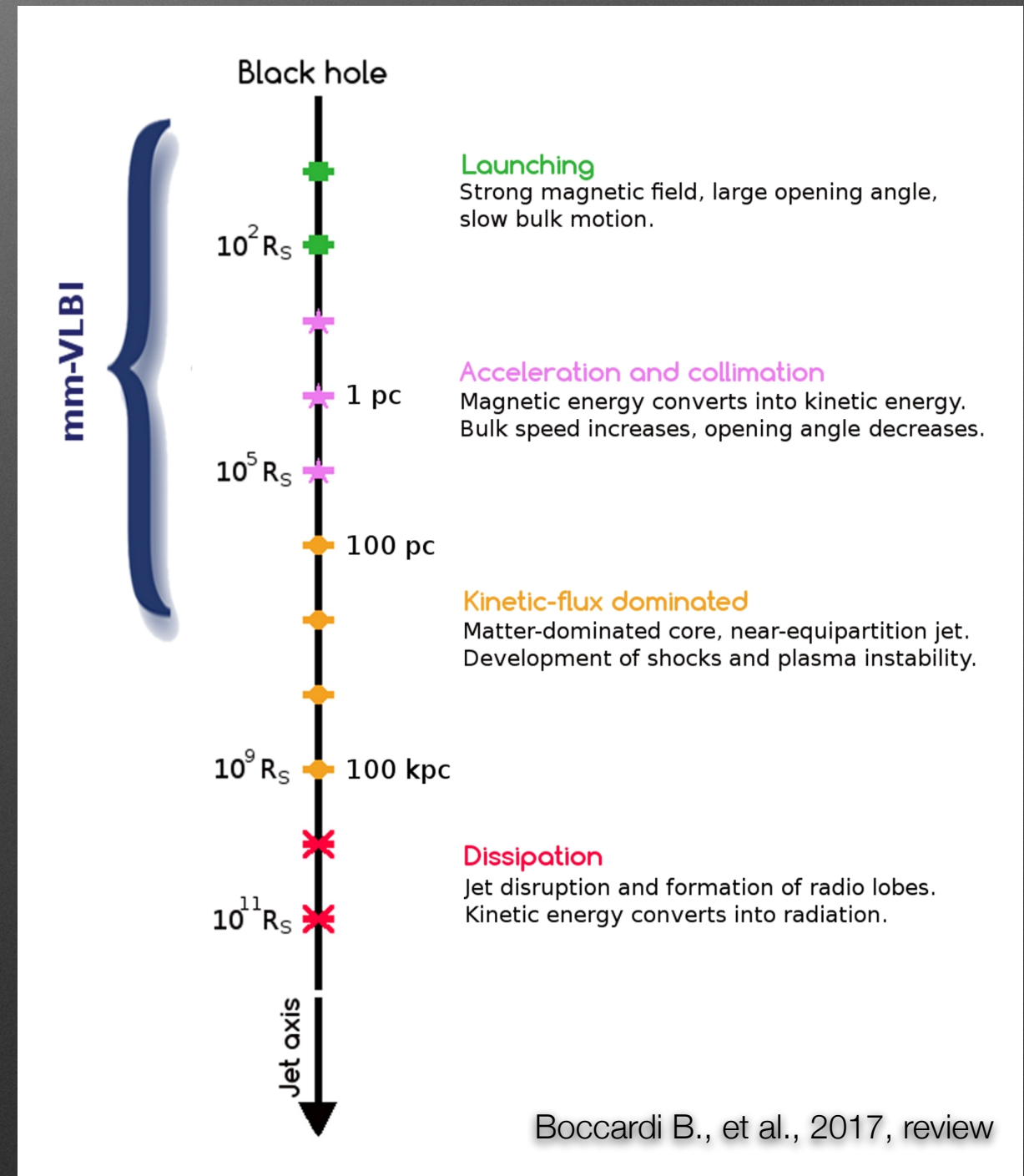
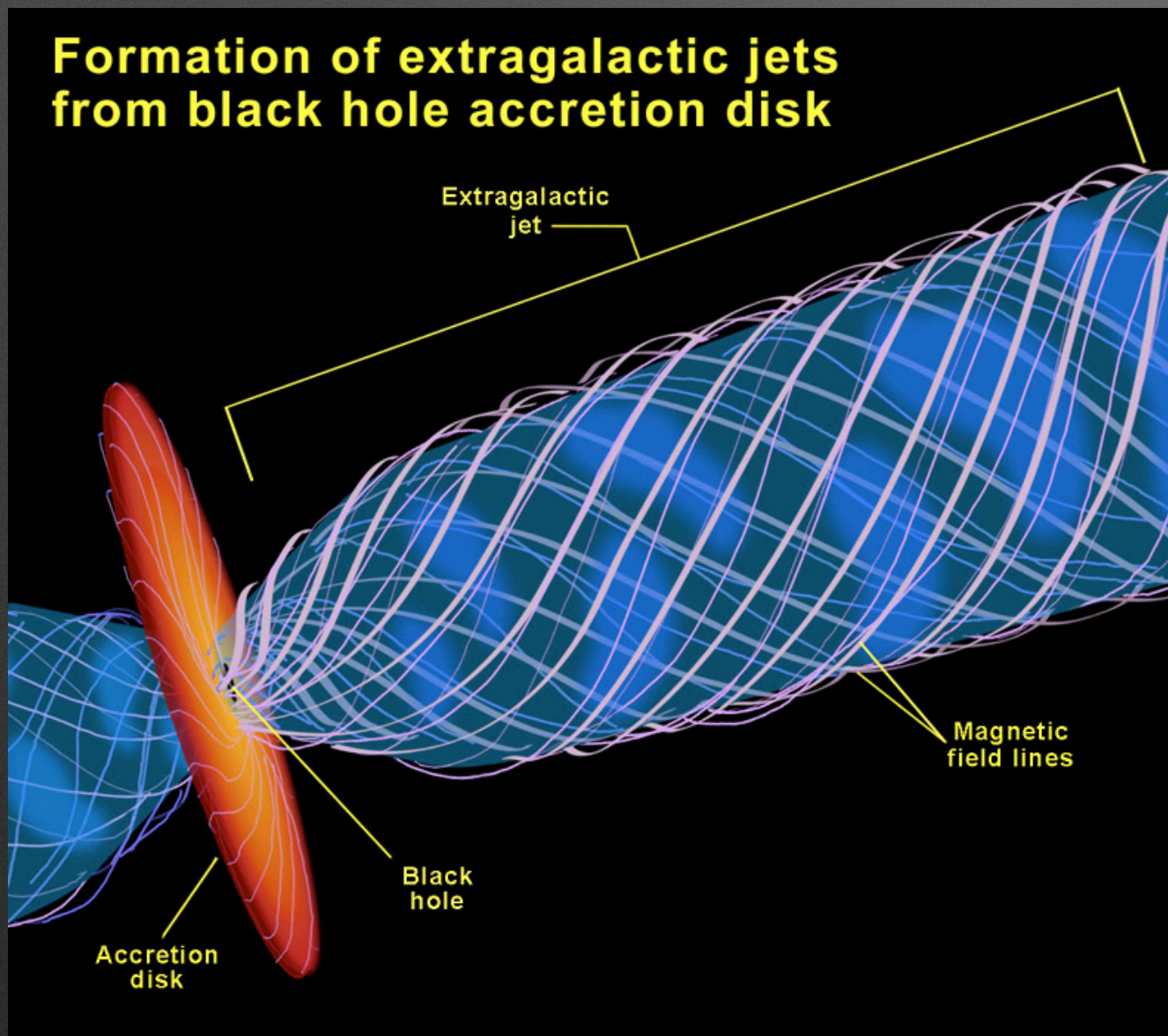
How jets are formed?

How are they accelerated up to Lorentz factors of tens, remaining highly collimated till far distances?

Blandford and Znajek, 1977

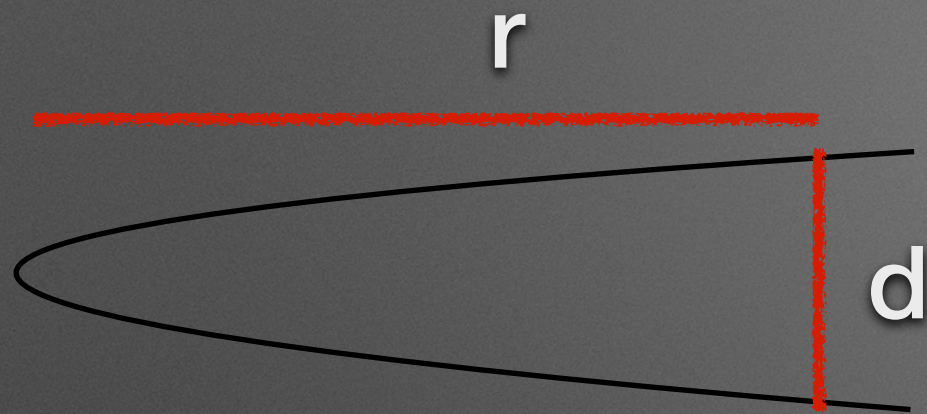
Blandford and Payne, 1982

Fundamental unit is Schwarzschild radius $R_S = 2GM_{BH}/c^2$



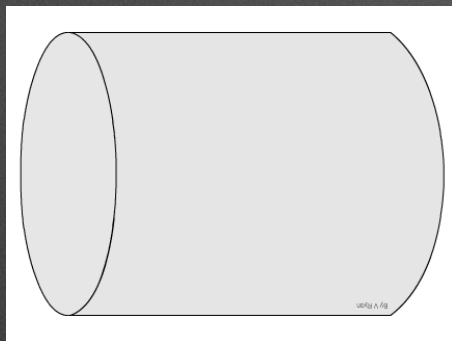
Jets shape changes with magnetization

$$d \propto r^k$$

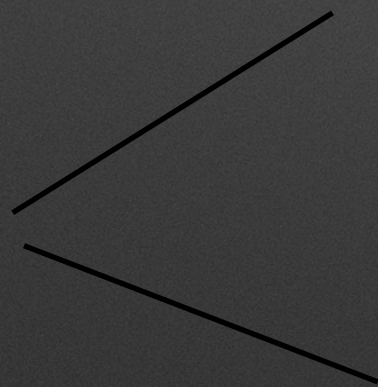


Parabola - the jet is accelerated

$$K = 0.5$$



Cylinder- the jet is accelerated (higher collimation)

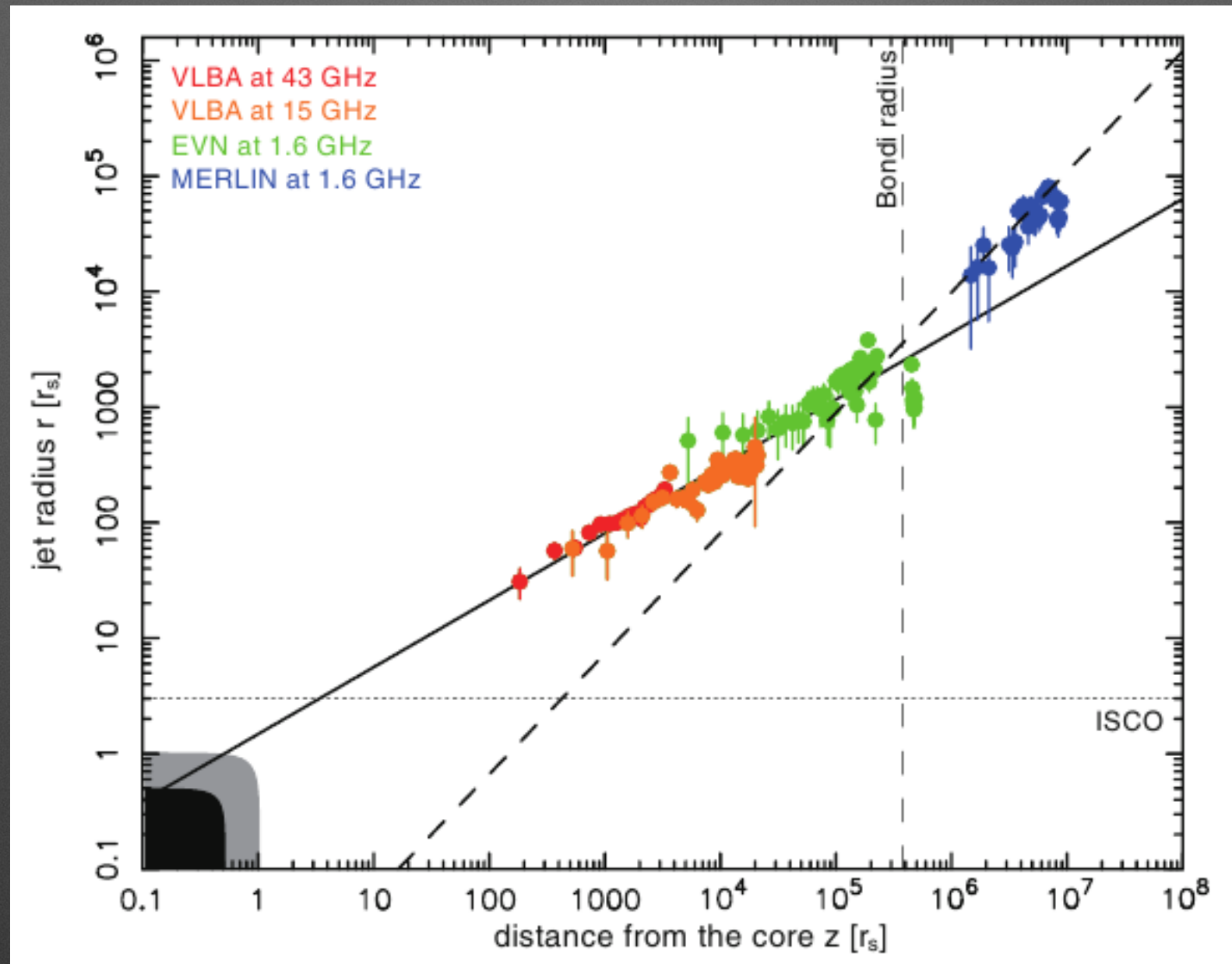


Cone- the jet expands freely

$$K = 1$$

.... and the external medium?

The radiogalaxy M87



Asada & Nakamura 2012

Transition from parabolic to conical shape at $\sim 10^5 R_S$, in the proximity of HST-1 and the Bondi radius.

Change in the External Pressure Profile

The Unified Model (Antonucci, Urry and Padovani, 90's)

RADIO QUIET AGN : Seyfert galaxies, Radio quiet quasars

RADIO LOUD AGN : Radiogalaxies, Blazars

Radiogalaxies

Different radio power and morphology
(Fanaroff & Riley, 1974)

FRII

$$P_{1.4GHz} > 10^{24.5} \text{ Watt / Hz}$$

FRI

$$P_{1.4GHz} < 10^{24.5} \text{ Watt / Hz}$$

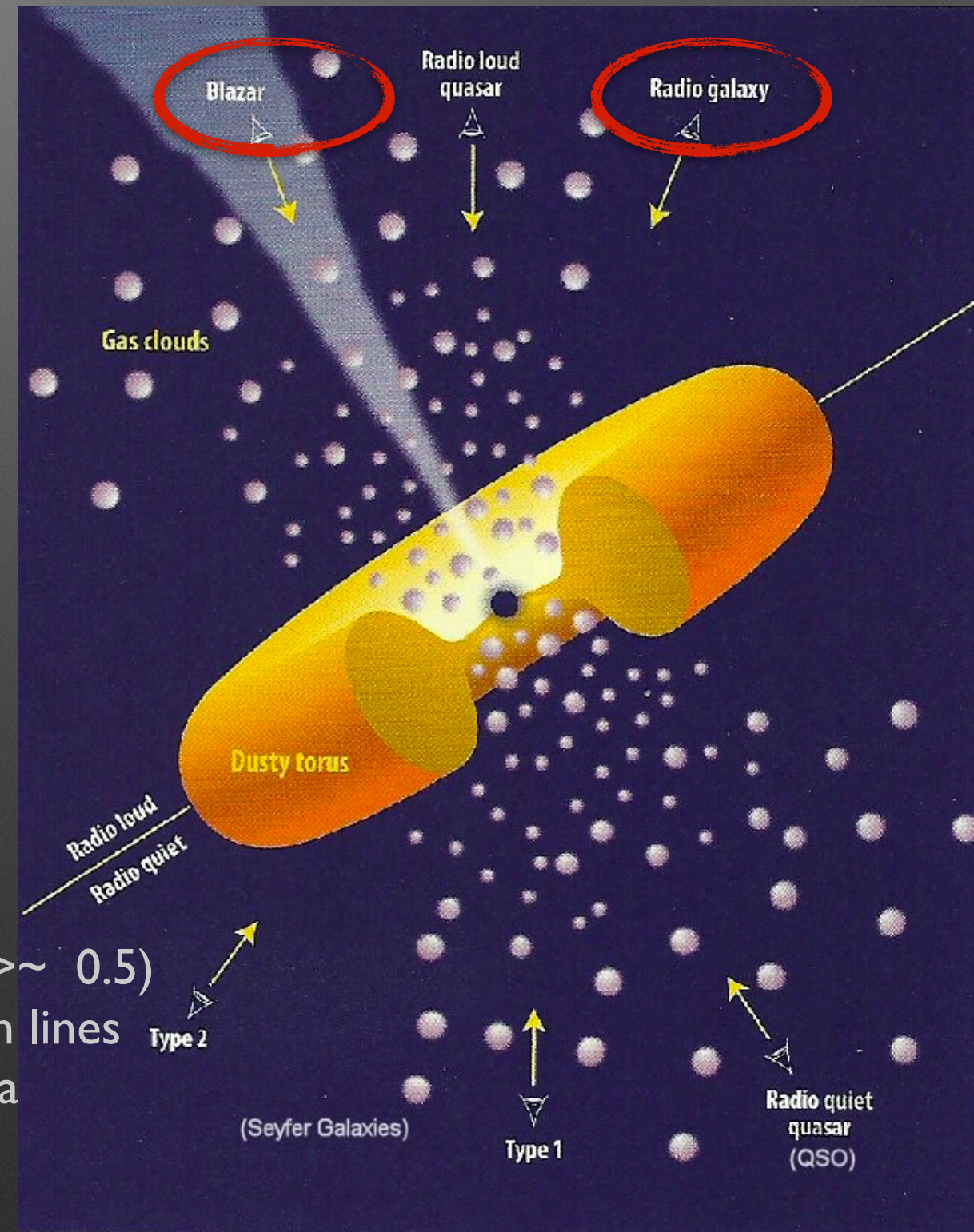
Blazars

BL LAC

- less luminous
- at smaller redshift ($z < \sim 0.1$)
- weak or no lines in their optical spectra

FSRQ

- more luminous
- at higher redshift ($z > \sim 0.5$)
- strong broad emission lines in their optical spectra



A transition from parabolic to conical shape as a common effect in nearby AGN jets

Y. Y. Kovalev^{1,2,3*}, A. B. Pushkarev^{4,1}, E. E. Nokhrina², A. V. Plavin^{1,2},
V. S. Beskin^{1,2}, A.V. Chernoglazov^{1,2}, M. L. Lister⁵, T. Savolainen^{6,7,3}

¹Lebedev Physical Institute, Leninsky prosp. 53, Moscow, 119991, Russia

²Moscow Institute of Physics and Technology, Dolgoprudny, Institutsky per., 9, Moscow region, 141700, Russia

³Max-Planck-Institut für Radioastronomie, Auf dem Hügel 69, 53121 Bonn, Germany

⁴Crimean Astrophysical Observatory, Nauchny 298688, Crimea, Russia

⁵Department of Physics and Astronomy, Purdue University, 525 Northwestern Avenue, West Lafayette, IN 47907, USA

⁶Aalto University Metsähovi Radio Observatory, Metsähovintie 114, 02540 Kylmälä, Finland

⁷Aalto University Department of Electronics and Nanoengineering, PL 15500, 00076, Aalto, Finland

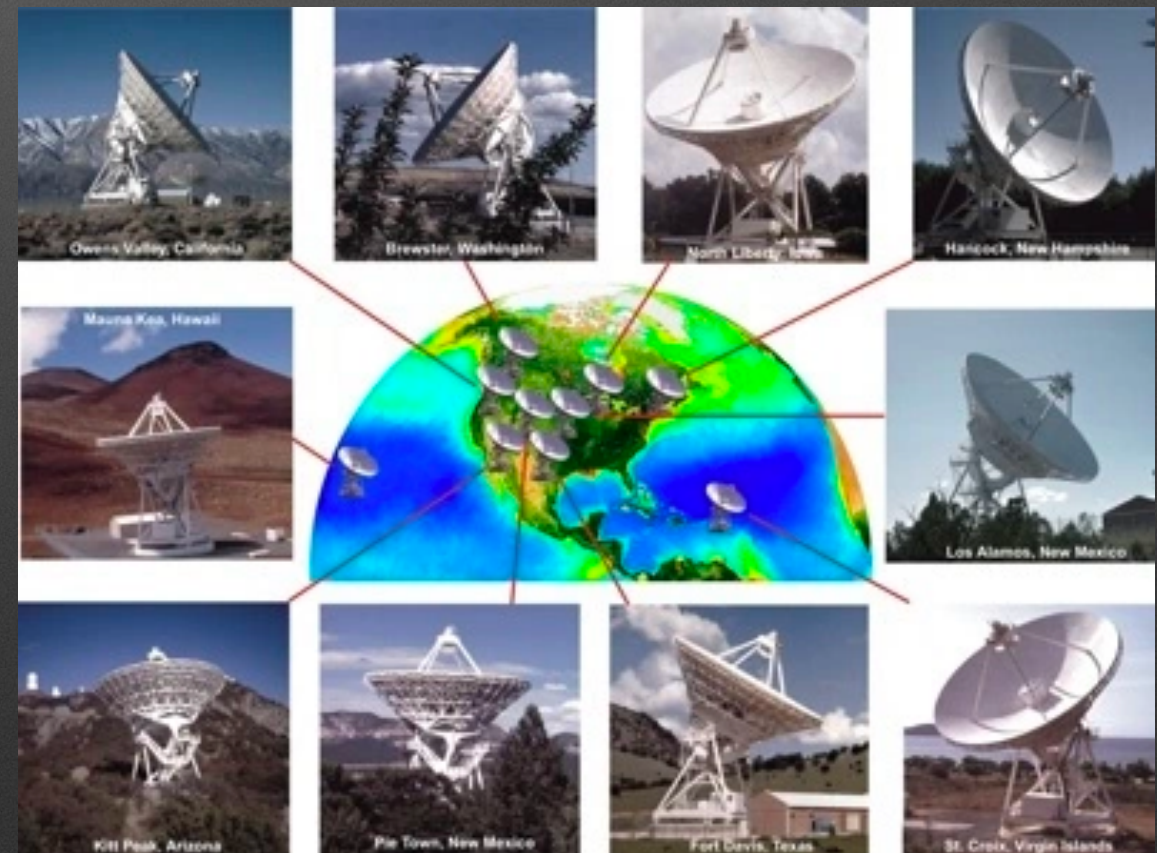
Accepted 2020 April 18. Received 2020 April 18; in original form 2019 June 23

Sample: 367 AGN

Data: 15 GHz VLBA stacked images (**MOJAVE**)
+ single epoch 1.4 GHz VLBA obs.

Resolution ~ 1 mas

At $z=1 \rightarrow 1 \text{ mas} \sim 8 \text{ pc}$



STEPS

1. Automated search of candidates with a change in the jet geometry

They divided jets lengths into two parts in proportion 1:1, 1:2, and 1:3 in logarithmic scale, to perform a double power law fit of the jet width as a function of distance:

$$d \propto r^k$$

RESULTS:

They drop 36 AGN from the original 367 analyzed because of:

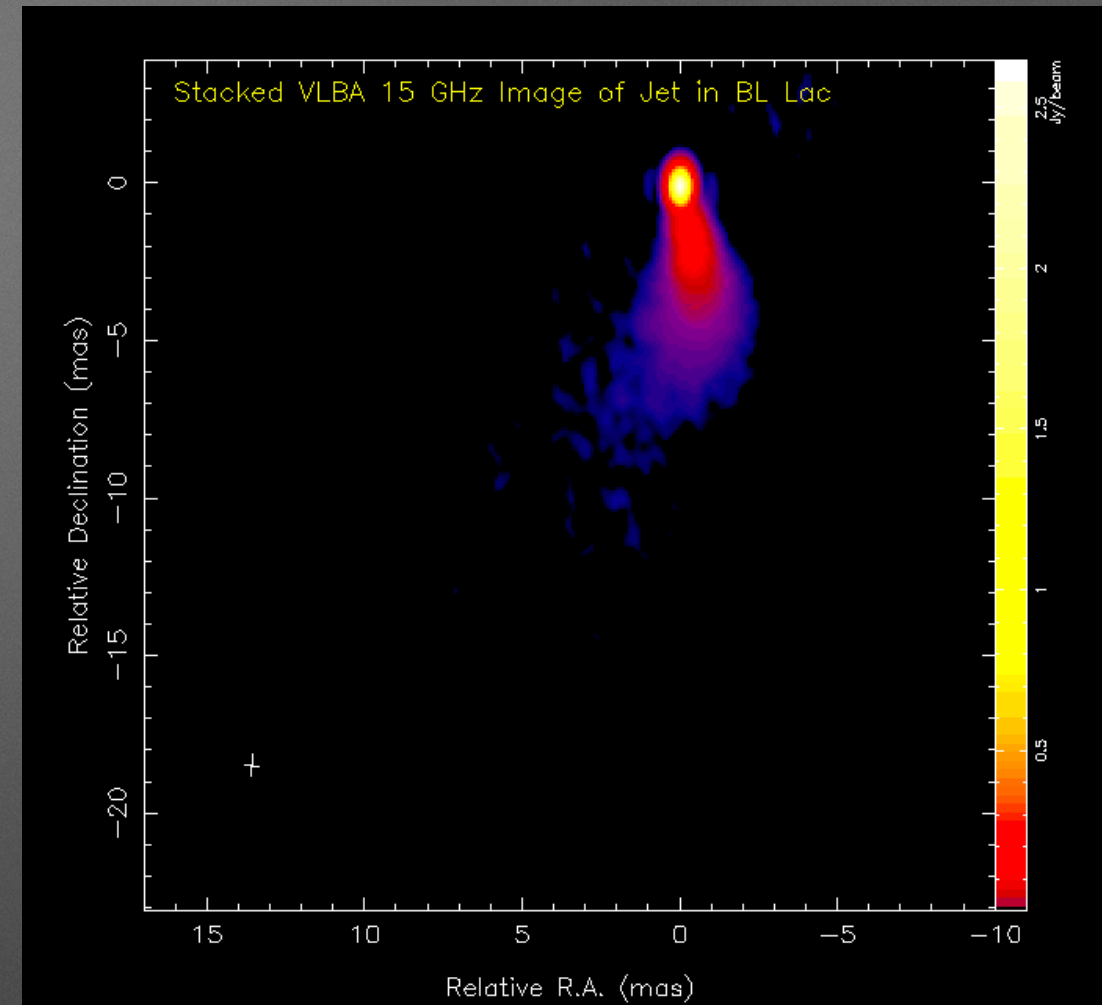
- i) jet bending (non optimal ridge line)
- ii) Large gaps in the emission
- iii) Too short jet length
- iv) Low intensity region not captured properly

10 jets out of 331 show a transition from $K \sim 0.5$ to $k \sim 1$

All of them at $z < 0.07$ (better than 1 pc resolution)

10 out of 29 nearby ($z < 0.07$) jets observed in MOJAVE

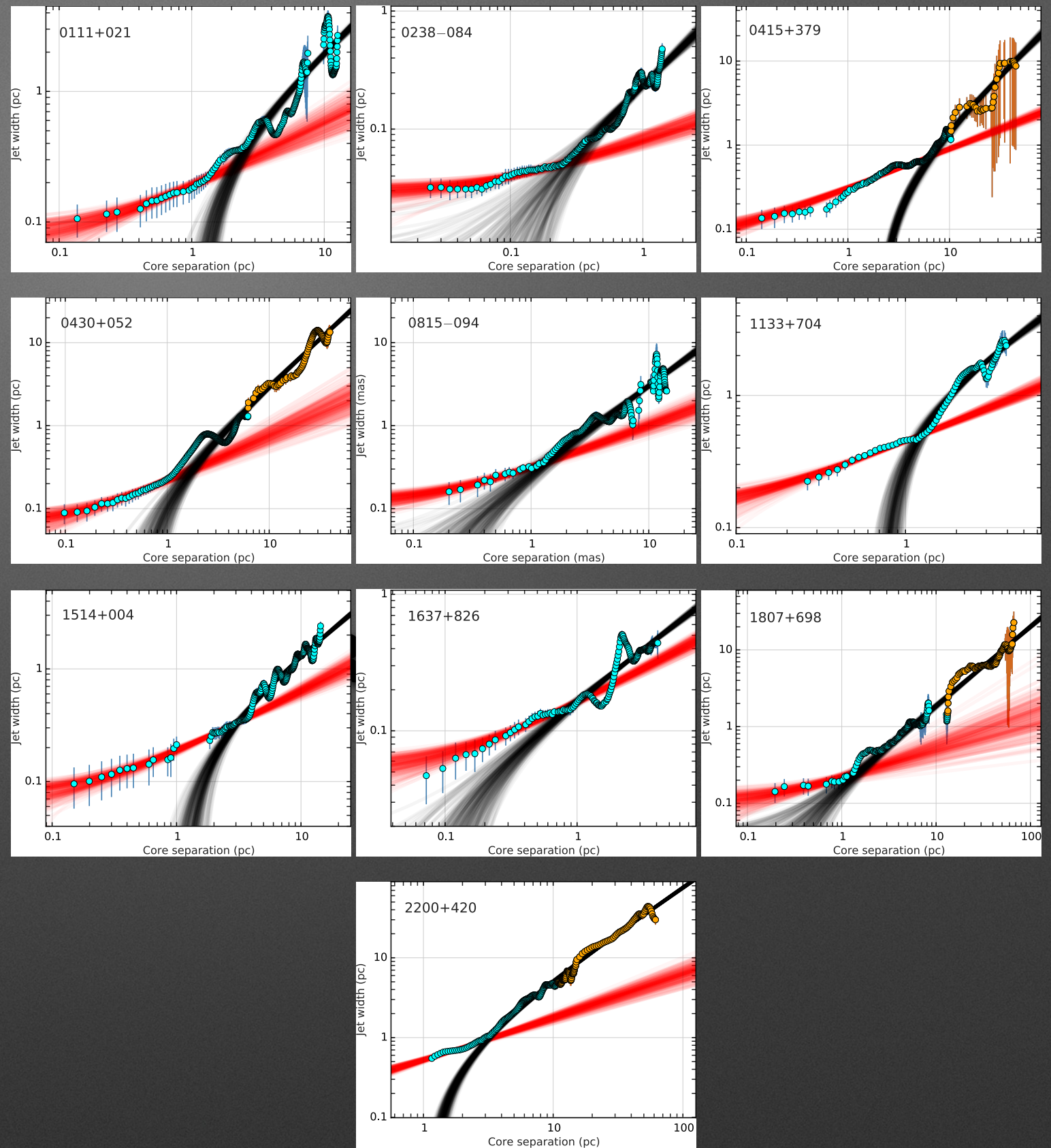
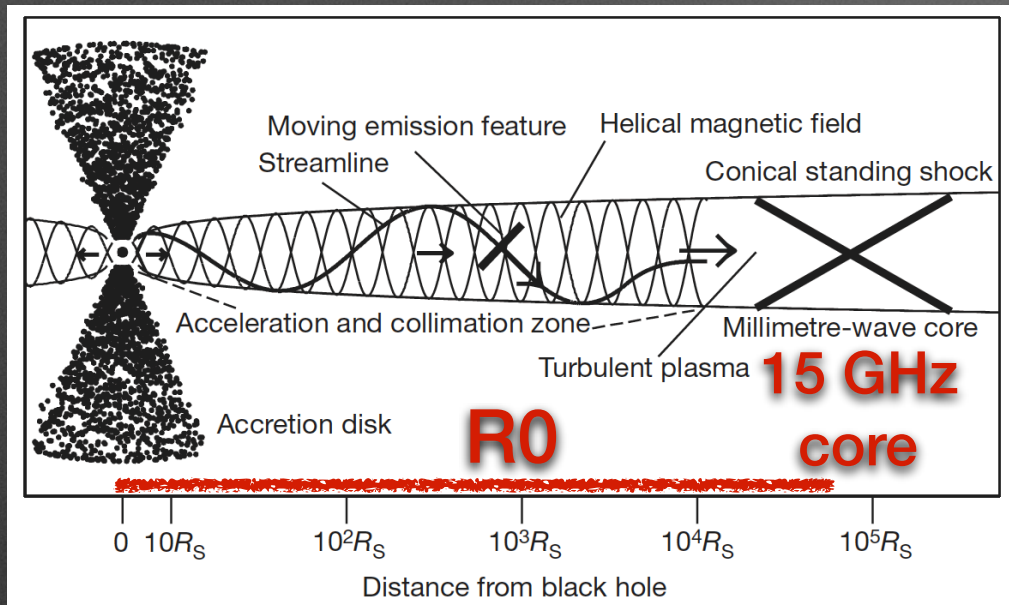
For the rest: $k \sim 1$ (conical shape)



2. More rigorous fitting of the jet shape for the 10 AGN

$$d = a_1(r + r_0)^{k1}$$

$$d = a_2(r + r_1)^{k2}$$



They fit these dependencies using Bayesian modelling using the NUTS MCMC sampler based on the gradient of the log posterior density

Figure 1. Jet profiles with an indication of transition from parabolic to conical shape in ten well resolved nearby active galaxies. The dependence of the jet width on projected distance from the apparent jet base is shown. The cyan and orange dots show measurements at 15 GHz and 1.4 GHz, respectively. The red and black stripes represent Monte Carlo fits for jet regions before and beyond the jet shape transition region, respectively. The projected distance is shown in pc for targets with known redshift and in mas for 0815–094 which has no redshift information. General properties of these AGN are presented in [Table 1](#), parameters of the fits — in [Table 2](#), parameters of the shape transition region — in [Table 4](#).

Source	Band	r_{\min} (mas)	r_{\max} (mas)	a_1 (pc $^{1-k_1}$)	a_1 (mas $^{1-k_1}$)	(pc)	r_0 (mas)	k_1
0111+021	U	0.2	1.5	0.179 ± 0.010	0.188 ± 0.011	0.143 ± 0.085	0.157 ± 0.093	0.497 ± 0.077
0238-084	U	0.3	2.5	0.078 ± 0.007	0.319 ± 0.046	0.074 ± 0.038	0.740 ± 0.380	0.391 ± 0.048
0415+379	U	0.2	6.0	0.305 ± 0.011	0.313 ± 0.011	0.042 ± 0.020	0.044 ± 0.021	0.468 ± 0.026
0430+052	U	0.2	2.0	0.202 ± 0.015	0.245 ± 0.020	0.122 ± 0.071	0.188 ± 0.109	0.556 ± 0.070
0815-094	U	0.2	1.0	...	0.294 ± 0.015	...	0.163 ± 0.048	0.527 ± 0.044
1133+704	U	0.3	1.5	0.437 ± 0.013	0.464 ± 0.014	0.061 ± 0.046	0.069 ± 0.052	0.528 ± 0.040
1514+004	U	0.2	3.5	0.171 ± 0.011	0.171 ± 0.011	0.189 ± 0.088	0.189 ± 0.088	0.564 ± 0.048
1637+826	U	0.2	3.0	0.155 ± 0.005	0.223 ± 0.010	0.098 ± 0.044	0.204 ± 0.092	0.506 ± 0.041
1807+698	U	0.2	1.4	0.207 ± 0.016	0.210 ± 0.016	0.130 ± 0.089	0.133 ± 0.091	0.388 ± 0.087
2200+420	U	0.9	2.0	0.505 ± 0.029	0.449 ± 0.027	0.087 ± 0.096	0.067 ± 0.074	0.537 ± 0.057

Source	Band	r_{\min} (mas)	r_{\max} (mas)	a_2 (pc $^{1-k_2}$)	a_2 (mas $^{1-k_2}$)	(pc)	r_1 (mas)	k_2
0111+021	U	1.5	14.0	0.252 ± 0.031	0.254 ± 0.031	-1.126 ± 0.181	-1.237 ± 0.199	0.934 ± 0.054
0238-084	U	2.5	14.1	0.252 ± 0.021	0.228 ± 0.047	-0.069 ± 0.067	-0.690 ± 0.670	1.052 ± 0.081
0415+379	UL	6.0	60.8	0.123 ± 0.019	0.122 ± 0.019	-2.043 ± 0.100	-2.151 ± 0.105	1.175 ± 0.046
0430+052	UL	2.0	121.9	0.229 ± 0.022	0.216 ± 0.021	-0.500 ± 0.188	-0.769 ± 0.289	1.131 ± 0.027
0815-094	U	1.0	14.3	...	0.282 ± 0.033	...	-0.085 ± 0.097	1.032 ± 0.049
1133+704	U	1.5	5.1	0.921 ± 0.057	0.941 ± 0.058	-0.753 ± 0.083	-0.857 ± 0.094	0.828 ± 0.047
1514+004	U	3.5	14.3	0.185 ± 0.010	0.185 ± 0.010	-1.167 ± 0.102	-1.167 ± 0.102	0.886 ± 0.022
1637+826	U	3.0	8.9	0.175 ± 0.007	0.213 ± 0.010	-0.089 ± 0.048	-0.185 ± 0.100	0.730 ± 0.029
1807+698	UL	1.4	85.2	0.179 ± 0.018	0.179 ± 0.018	-0.120 ± 0.188	-0.122 ± 0.192	1.023 ± 0.025
2200+420	UL	2.0	49.0	0.433 ± 0.016	0.447 ± 0.016	-1.142 ± 0.093	-0.885 ± 0.072	1.124 ± 0.009

Source	d_{break} (mas)	d_{break} (pc)	$r_{\text{break, app}}^{\text{proj}}$ (mas)	$r_{\text{break}}^{\text{proj}}$ (mas)	$r_{\text{break}}^{\text{proj}}$ (pc)	$r_{\text{break}}^{\text{deproj}}$ (pc)	Stationary jet feature	
(1)	(2)	(3)	(4)	(5)	(6)	(7)	(8)	
UGC 00773 (B)	0111+021	0.30 ± 0.03	0.28 ± 0.03	2.46 ± 0.27	2.62 ± 0.29	2.38 ± 0.26	27.31	Y
NGC 1052 (G)	0238-084	0.53 ± 0.05	0.05 ± 0.01	2.93 ± 0.57	3.73 ± 0.65	0.37 ± 0.06	0.49	Y
1H 0323+342 (NLSy1)	0321+340	1	1.16	10	10.04	11.64	106.07	Y ^a
3C111 (G)	0415+379	0.78 ± 0.03	0.74 ± 0.03	7.03 ± 0.50	7.07 ± 0.50	6.72 ± 0.47	29.00	...
3C120 (G)	0430+052	0.45 ± 0.06	0.29 ± 0.04	2.67 ± 0.40	2.85 ± 0.41	1.85 ± 0.27	5.77	...
TXS 0815-094 (B)	0815-094	0.37 ± 0.05	...	1.37 ± 0.30	1.54 ± 0.30
MrK 180 (B)	1133+704	0.57 ± 0.02	0.50 ± 0.02	1.39 ± 0.09	1.46 ± 0.10	1.29 ± 0.09	14.80	...
M87 (G)	1228+126	13.00 ± 0.50	1.20 ± 0.04	...	131 ± 6	10.50 ± 0.46	43.41	Y ^b
PKS 1514+00 (G)	1514+004	0.34 ± 0.02	0.34 ± 0.02	3.10 ± 0.22	3.39 ± 0.30	3.39 ± 0.30	13.10	Y
NGC 6251 (G)	1637+826	0.32 ± 0.02	0.16 ± 0.01	1.92 ± 0.26	2.13 ± 0.28	1.02 ± 0.13	3.30	Y
3C 371 (B)	1807+698	0.26 ± 0.04	0.25 ± 0.04	1.53 ± 0.33	1.67 ± 0.34	1.63 ± 0.33	12.83	Y
BL Lac (B)	2200+420	0.74 ± 0.03	0.95 ± 0.04	2.45 ± 0.10	2.52 ± 0.13	3.25 ± 0.16	24.57	...

From the core From the BH

Analysis and comparison for possible biases

$$d = a_1(r + r_0)^{k1}$$

For $r=0$ we obtain the apparent size of the 15 GHz core (**dc_MC**) to compare with the core size obtained from model fit components (**dc_uv**, Lister et al., 2019)

Source	d_c^{MC} (mas)	d_c^{uv} (mas)	r_0^{MC} (mas)	r_0^{CS} (mas)
(1)	(2)	(3)	(4)	(5)
0111+021	0.075 ± 0.025	0.079 ± 0.030	0.157 ± 0.093	0.159 ± 0.050
0238-084	0.282 ± 0.067	0.284 ± 0.042	0.740 ± 0.380	...
0415+379	0.073 ± 0.017	0.075 ± 0.008	0.044 ± 0.021	0.275 ± 0.050
0430+052	0.096 ± 0.034	0.182 ± 0.014	0.188 ± 0.109	0.051 ± 0.050
0815-094	0.113 ± 0.020	0.062 ± 0.041	0.163 ± 0.048	...
1133+704	0.116 ± 0.049	0.089 ± 0.048	0.072 ± 0.056	...
1514+004	0.067 ± 0.018	0.043 ± 0.027	0.189 ± 0.088	...
1637+826	0.100 ± 0.025	0.069 ± 0.004	0.204 ± 0.092	0.198 ± 0.050
1807+698	0.096 ± 0.031	0.067 ± 0.007	0.133 ± 0.091	0.240 ± 0.050
2200+420	0.105 ± 0.064	0.044 ± 0.003	0.067 ± 0.074	0.090 ± 0.050

Possible causes:

- unresolved jets near the core (radiogalaxies less affected)
- uncertainties in core position \rightarrow imperfect alignment of images while performing the sacking



They excluded jet width measurements at $r < 0.5$ mas for the 321 sources + $r < 0.9$ mas for BLLAC from

Analysis and comparison for possible biases

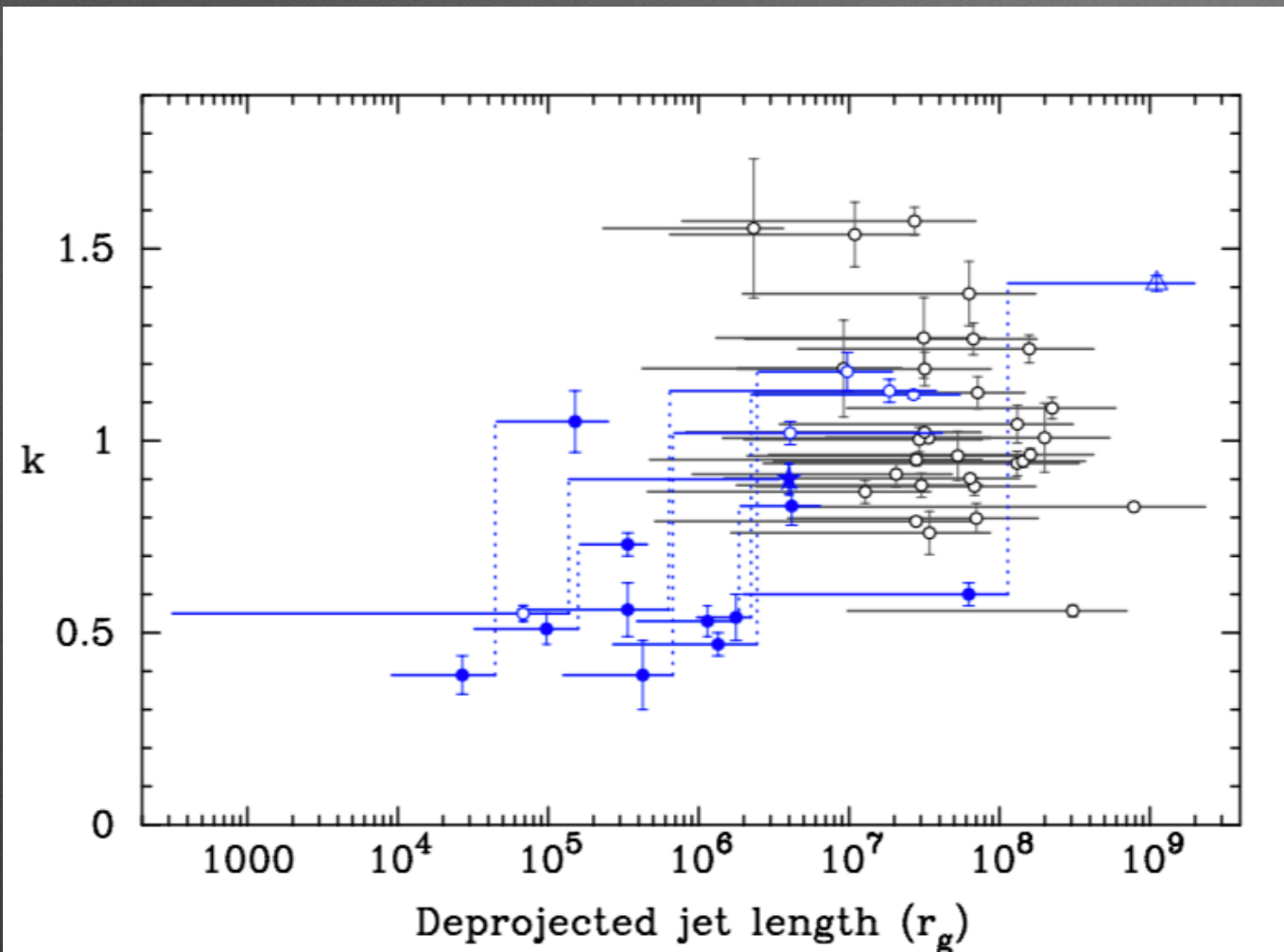
$$d = a_1(r + r_0)^{k_1}$$

For $r=0$ we obtain the apparent size of the 15 GHz core (**dc_MC**) to compare with the core size obtained from model fit components (**dc_uv**, Lister et al., 2019)

Source (1)	d_c^{MC} (mas) (2)	d_c^{uv} (mas) (3)	r_0^{MC} (mas) (4)	r_0^{CS} (mas) (5)
0111+021	0.075 ± 0.025	0.079 ± 0.030	0.157 ± 0.093	0.159 ± 0.050
0238-084	0.282 ± 0.067	0.284 ± 0.042	0.740 ± 0.380	...
0415+379	0.073 ± 0.017	0.075 ± 0.008	0.044 ± 0.021	0.275 ± 0.050
0430+052	0.096 ± 0.034	0.182 ± 0.014	0.188 ± 0.109	0.051 ± 0.050
0815-094	0.113 ± 0.020	0.062 ± 0.041	0.163 ± 0.048	...
1133+704	0.116 ± 0.049	0.089 ± 0.048	0.072 ± 0.056	...
1514+004	0.067 ± 0.018	0.043 ± 0.027	0.189 ± 0.088	...
1637+826	0.100 ± 0.025	0.069 ± 0.004	0.204 ± 0.092	0.198 ± 0.050
1807+698	0.096 ± 0.031	0.067 ± 0.007	0.133 ± 0.091	0.240 ± 0.050
2200+420	0.105 ± 0.064	0.044 ± 0.003	0.067 ± 0.074	0.090 ± 0.050

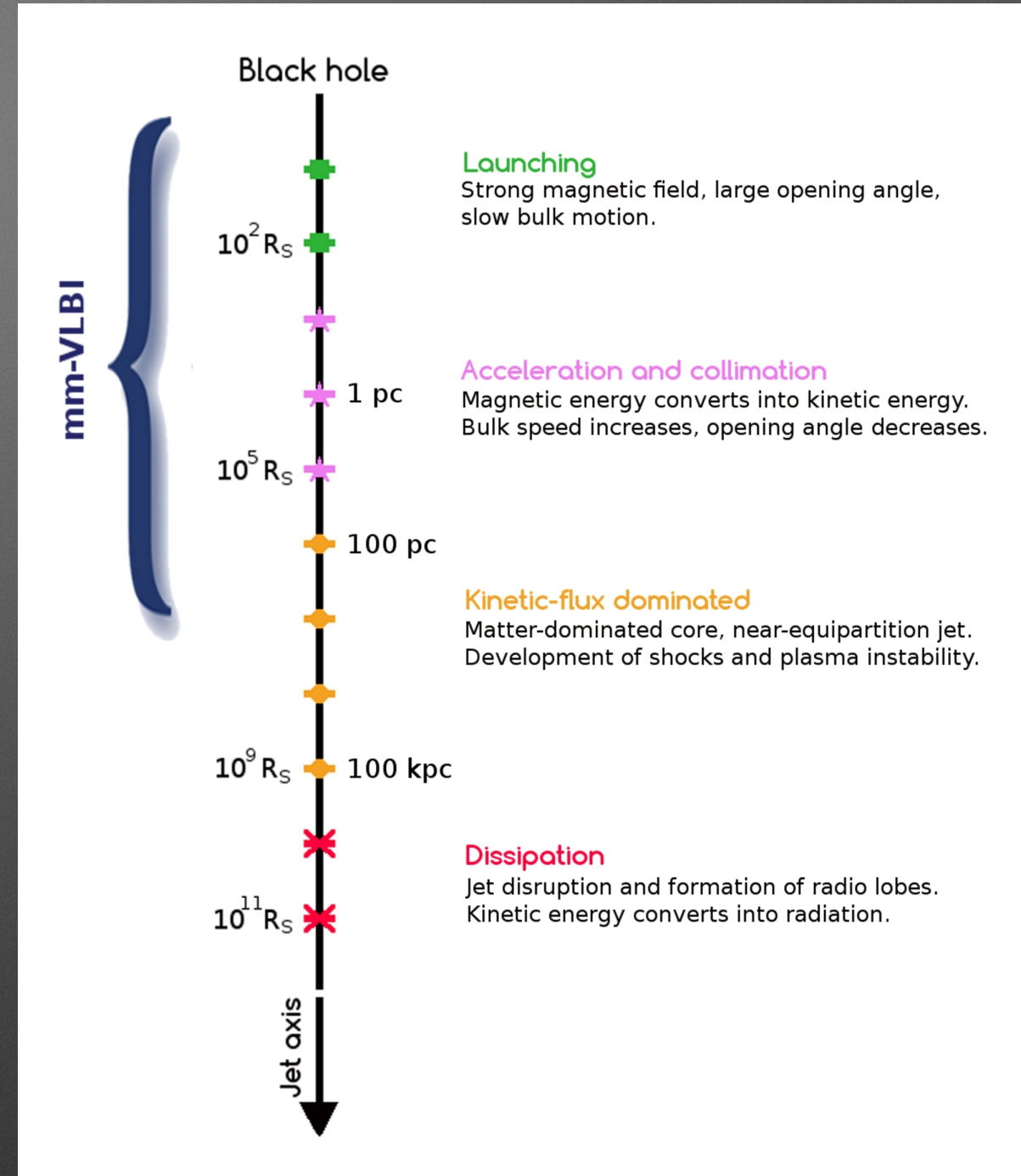
From core-shift measurements between 15 and 8 GHz, assuming $r \propto \nu^{-1}$ (Pushkarev+2012)

Deprojected position of the jet break



↓
Uncertainties coming from
BH Mass estimation and Viewing Angles

↓
Using reverberation mapping and BLR motion + stellar and gas kinematics for closest sources (data taken from other papers)



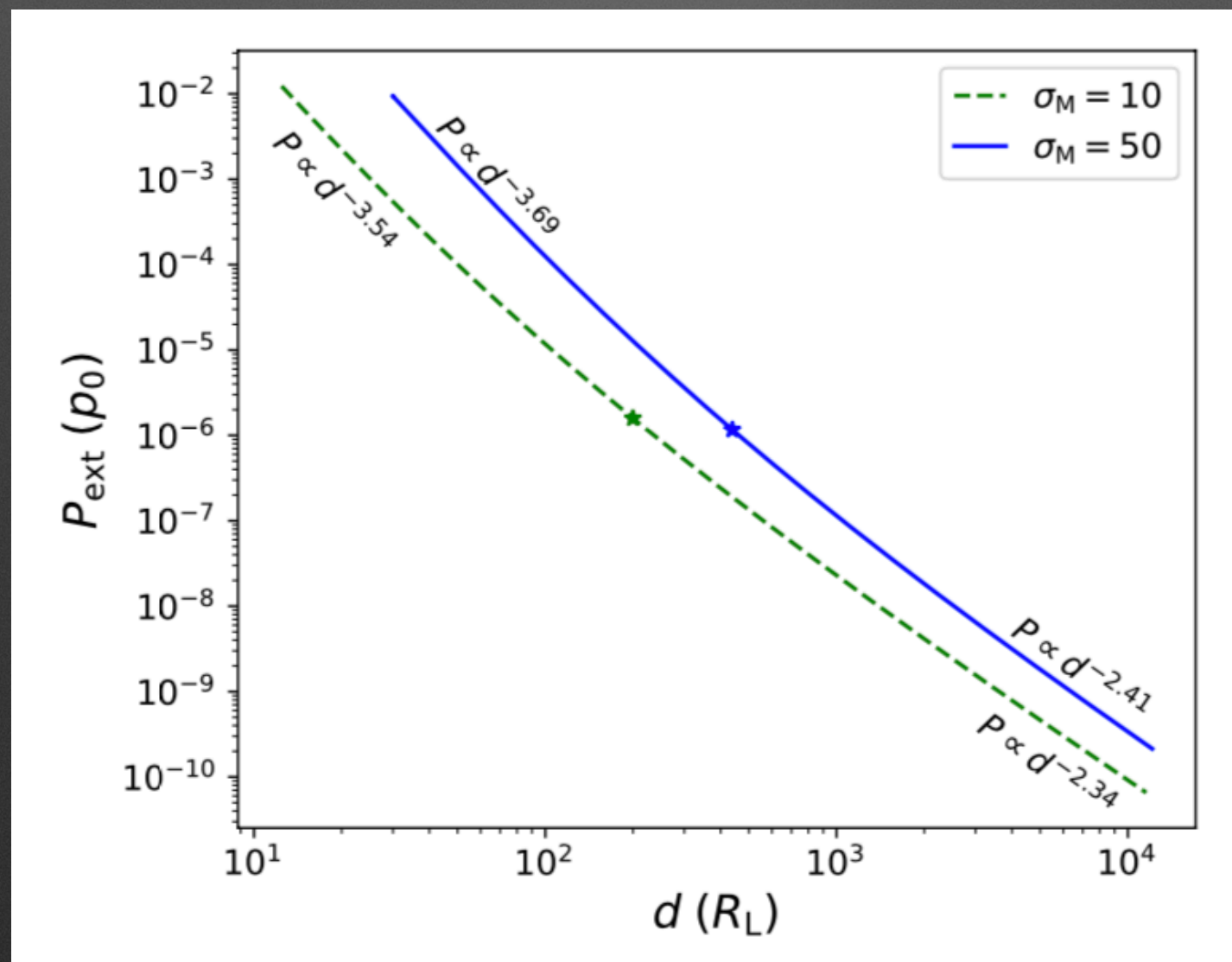
Semi-Analytical model

Equations from [Beskin et al. \(2017\)](#) : Bernulli equation + Grad-Shafranov equation

Knowing 5 integrals of motion (Energy and Angular Momentum flux, electric potential which connects with angular velocity, entropy, and particle-to-magnetic flux ration)

To determine the internal structure of axisymmetric stationary jets

After some assumptions (e.g. cylindrical jet), the considered system of the equations is valid for both magnetically and particle dominated flows with the solution depending only on **external Pressure**



$$P \propto d^{-3.7} \quad (8)$$

closer to the jet base to

$$P \propto d^{-2.4} \quad (9)$$

For magnetisation = 50

We assume the equilibrium between jet and ambient medium pressure. In order to model a jet shape break position along the jet, we need to introduce the exerted pressure dependence on r , which we choose in the power law form

$$P_{\text{ext}} = P_0 \left(\frac{r}{r_0} \right)^{-b} . \quad (10)$$

Such a pressure profile is consistent with Bondi flow (Quataert & Narayan 2000; Shcherbakov 2008; Narayan & Fabian 2011) having $b \in (1.5; 2.5)$ for different models, with the limiting value 2.5 for classical supersonic Bondi flow.

Pressure profile consistent with Bondi flow

With $b=2$, solving eq. 8, 9, 10:

$$d \propto r^{0.54} .$$

Accordingly, for large distances

$$d \propto r^{0.83} .$$

Change of the jet shape without changing external Pressure profile (Bondi pressure profile)

Different to what we have in M87 (Asada & Nakamura 2012)

Magnetization

In this subsection we check whether the break in a jet shape corresponds to the transition from the magnetically-dominated into the equipartition regime. The jet magnetization is defined as the ratio of Poynting flux

$$\mathbf{S} = \frac{c}{4\pi} \mathbf{E} \times \mathbf{B} \quad (13)$$

to particle kinetic energy flux

$$\mathbf{K} = \gamma m c^2 n \mathbf{u}_p, \quad (14)$$

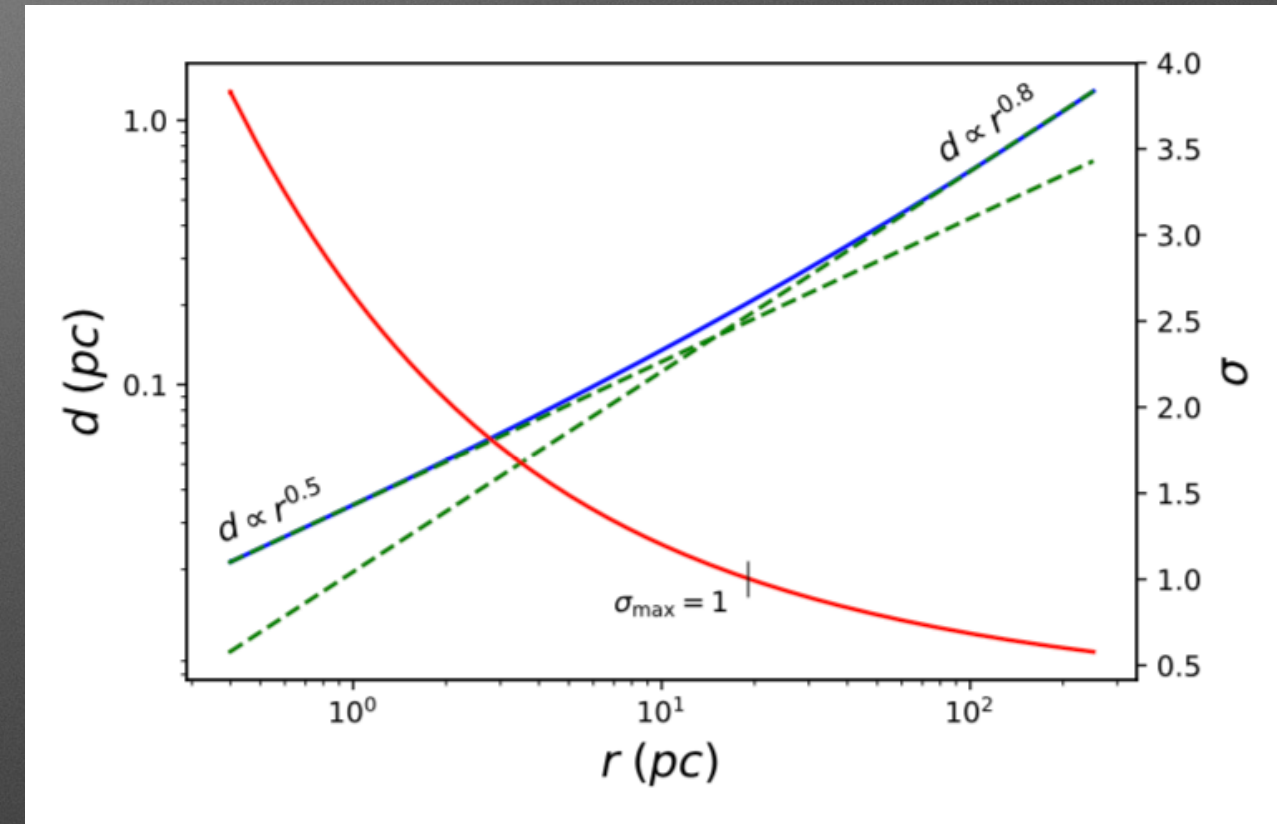
where n is particle number density in the jet proper frame. Using the standard expressions for ideal MHD velocities and electric and magnetic fields, one obtains the following expression for the magnetization:

$$\sigma = \frac{|\mathbf{S}|}{|\mathbf{K}|} = \frac{\Omega_F I}{2\pi c \gamma \mu \eta}. \quad (15)$$

Using the definitions of bulk Lorentz factor γ and total current I , we rewrite it as

$$\sigma = \Omega_F \frac{L - \Omega_F r_{\perp}^2 E / c^2}{E - \Omega_F L - \mathcal{M}^2 E}. \quad (16)$$

In order to check σ along the jet, we calculate the maximal magnetization across the jet for each given distance r .



Conclusions

They performed an automated search for jet shape transition in 367 AGN from MOJAVE sample using 15 and 1.4 GHz VLBA data

10 out of 331 show such a transition, from parabolic to conical shape; the rest have conical shape. All 10 are at $z < 0.07$, except for 0815-094 whose redshift is unknown.

6 Radiogalaxies and 6 BLLAC objects: A transition from parabolic to conical shape may be a general property of AGN jets.

The deprojected distance of the breaking point from the nucleus is typically 10 pc ($10^5 - 10^6 R_g$, which corresponds to the typical Bondi Radius).

The transition occurs when the plasma kinetic energy flux becomes equal to the Poynting energy flux, IF the ambient medium pressure is assumed to be governed by Bondi accretion

The well know effect of apparent core-shift with frequency due to synchrotron self-absorption does not follow $r \propto \nu^{-1}$ all the way up to the jet apex since -1 is expected in case of conical shape